Received 6 June 2022; revised 10 August 2022; accepted 12 August 2022. Date of publication 19 August 2022; date of current version 2 September 2022.
The review of this article was arranged by Editor G. I. Ng.

Digital Object Identifier 10.1109/JEDS.2022.3200120

Impact of AlGaN Barrier Thickness and Substrate Material on the Noise Characteristics of GaN HEMT

ANWAR JARNDAL (Senior Member, IEEE), ARIVAZHAGAN L, EQAB ALMAJALI, SOHAIB MAJZOUB (Senior Member, IEEE), TALAL BONNY, AND SOLIMAN MAHMOUD (Senior Member, IEEE)

Electrical Engineering Department, University of Sharjah, Sharjah, UAE

CORRESPONDING AUTHOR: A. JARNDAL (e-mail: ajarndal@sharjah.ac.ae)

This work was supported by the University of Sharjah, Sharjah, UAE.

ABSTRACT In this paper, the impact of AlGaN barrier thickness (t_{AlGaN}) and substrate leakage on the noise conductance and noise figure in GaN High Electron Mobility Transistor (HEMT) is investigated. The investigation and analysis in this paper are targeting the Low Noise Amplifier (LNA) applications. The noise analysis is carried out using Technology Computer-Aided Design (TCAD) physical simulator. Initially, the DC, RF, and noise simulations are validated against measurements of a GaN device. AlGaN barrier thickness (t_{AlGaN}) is varied and its impact on the minimum noise figure (NFmin) is analyzed. It is observed that the NFmin decreases with t_{AlGaN} reduction at the typical bias conditions of LNA. This observation on the impact of t_{AlGaN} on the NFmin follows Fukui's model, which states that the NFmin decreases with the increase in transconductance. In addition, the impact of the substrate material on noise performance is analyzed. The substrates used for the investigation are Silicon (Si) and Silicon Carbide (SiC). At 40 GHz, it is found that the noise conductance and the NFmin of GaN HEMT on SiC substrate is reduced by 13% and 12%, respectively, in comparison with GaN HEMT on Si substrate. This could be attributed to the lower gate-to-substrate capacitance of the GaN HEMT on SiC substrate.

INDEX TERMS LNA, AlGaN barrier, substrate leakage, noise figure.

I. INTRODUCTION

For RF, microwave and millimeter-wave (mm-Wave) receivers, the low noise amplifier (LNA) has become an essential component. Recently, there has been a huge demand for mm-Wave LNAs to cope with the fast-growing mm-Wave wireless communications market that arose from the rising demand for high data rates. The LNA is usually used to amplify weak received power without degrading the signal-to-noise ratio (SNR). The important figure of merit for any LNA is the noise figure (NF), which represents the ratio of the SNR at the input to the SNR at the output of the amplifier. The NF of the receiver depends mainly on the NF of its front-end LNA. The impedance matching and the biasing of the LNA have to be carefully chosen to ensure the best noise performance. The properties of the GaN HEMT technology like its high breakdown voltage and high frequency of operation, are favorable for the design of both power and low noise amplifiers. The GaN HEMT based LNAs can be operated at higher operating voltages compared to all other alternative technologies. To realize a GaN based LNA with good noise performance, it is inevitable to use a reliable GaN HEMT noise model. Most of the research on noise modelling of the GaN HEMT is based on equivalent circuit models [1], [2], [3], [4], [5], [6]. Physical modeling of GaN HEMT associated with studying the impact of changing physical parameters on the noise performance of the LNA has not been given enough consideration. Therefore, this work aims at investigating the impact of transistor

physics (material and structure) on the noise characteristics of the GaN-HEMT based LNA.

Recently, different techniques have been proposed in the literature for attaining low NF for the GaN HEMT. Graded channel AlGaN/GaN HEMT is reported in [7] to improve its NF as compared to the conventional AlGaN/GaN HEMT. A 50-nm T-gate graded channel HEMT is used to achieve a NF of 0.5 dB at 30 GHz. The lower NF of the graded channel HEMT is attributed to the improved gain and the lower gate capacitance of the device. In [8], the effect of barrier thickness and Al mole fraction on AlGaN barrier was studied for enhancement-mode GaN HEMT. The NF tends to increase with the barrier thickness and the Al mole fraction. It is due to that the parasitic resistance increases as AlGaN thickness increases [8]. However, relating NFmin with AlGaN thickness using parasitic resistance still needs more investigation. The effect of InGaN channel on the noise performance of GaN HEMT was reported in [9]. As compared to the GaN channel device, the InGaN channel device exhibited better noise performance as it owns a higher electron drift velocity. The effect of passivation on the device noise performance was investigated in [10]. It was observed that the passivation improves the noise performance of the GaN HEMT. The device with TiO_2 passivation exhibited reduced leakage and thus lower NF than the device with no passivation. In [11], it was shown that lowering access resistance, gate-source capacitance and gate contact resistance of the GaN HEMT, helped in achieving better noise performance. It was also observed in [12], that by reducing the gate-source spacing, the noise performance can be improved. Increasing the number of gate fingers and reducing the gate width of each finger was shown useful in reducing the gate resistance [13] and hence it was shown to improve the noise performance [12]. For T- and pi-gate GaN HEMT structures, variation of the NF with the gate bias in the C and X bands was studied in [14]. The recessed T-gate structure exhibited better noise performance when compared with the pi-gate structure. This could be attributed to the lower gate resistance of the T-gate device.

For LNA applications, the device behavior could be predicted based on current/voltage, S-parameters, and N-parameters measurements. Consequently, physics-related parameters could be extracted from these measurements. In contrast to the measurement-based technique, TCAD simulation can be used to extract and study more physical parameters such as carrier concentration, potential, electric field and leakage inside the LNA device [15]. Furthermore, the TCAD simulation assists the device manufacturer to design and develop transistors with better noise performance. TCAD is also useful in highlighting the intrinsic effect on the noise characteristics. Therefore, it could be effectively used for analyzing noise performance of GaN HEMT. On the other hand, the ADS SPICE based circuit simulation is shown very useful in studying the impact of the intrinsic and the extrinsic parameters on the noise performance of GaN HEMT. Most of the reported works on the noise performance

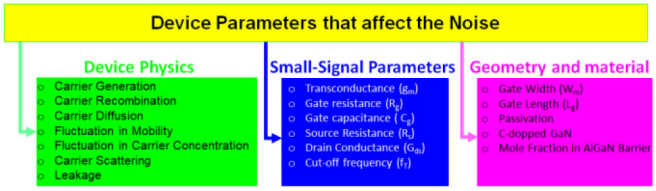

FIGURE 1. Device parameters that affect noise in a semiconductor device.

of AlGaN/GaN HEMT are experimental except the work reported in [8]. Despite the said work used the TCAD simulation, a detailed study of the physical parameters was neither included nor supported by device measurements. In addition to that, the AlGaN/GaN HEMT used in [8], is E-Mode MOSHEMT with N-polar technique and not E-Mode HEMT, nor a typical D-Mode GaN HEMT. The AlN back barrier is placed over the channel, which is not consistent with other several experimental works of placing the back barrier below the channel [16], [17], [18].

In this paper, the noise performance of GaN HEMT is investigated using TCAD simulation. The TCAD simulation is validated and supported by DC, RF and noise measurements of actual devices. TCAD simulation results for noise and RF performance are validated using measured data for the first time. Also, the simulation results show a very agreement with a physics-based analytical model.

II. IMPACT OF DEVICE PARAMETERS ON NOISE

Fig. 1 presents a list of device parameters that affect the noise level. The impact of device phenomena on noise is classified as (i) device physics, (ii) small-signal parameters and (iii) device geometry and material. As per the state of the art [19], [20], [21], [22], [23], [24], [25], [26], [27], [28], [29], the device physics that affect the noise in a semiconductor device are carrier diffusion, generation, recombination, fluctuation in mobility, leakage, presence of traps and scattering. The device parameters that affect the noise are transconductance (g_m), source-resistance (R_s), gate-resistance (R_g), gate-capacitance (C_g), drain-to-source conductance (g_{ds}) and cut-off frequency (f_t) [3]. The device geometry and material-related parameters that affect the noise are gate-width (W_g), gate-length (L_g), passivation material, mole fraction in AlGaN barrier and Carbon(C)-doped GaN buffer [19], [22], [30], [31]. Although these parameters affect the noise, most of them have not been optimized for noise reduction. In the state of the art of GaN HEMT, great effort has been exerted to improve breakdown voltage, cut-off frequency and reducing loss rather than reducing the noise at the device level [16], [32]. The only device-level optimizations are passivation and C-doped GaN buffer [22], [30], [31]. The remaining device material and geometry parameters are left open for further investigation to reduce noise at the device level. Furthermore, the relation between the noise and the physics behind the changes that occur in some of the device parameters is not yet well established in the open literature. For instance, in [3], it was

found that the noise figure increases as the gate width or the number of gate fingers are increased without providing clear physical justification for this observation. In order to debate this observation [3], Fukui's theory is briefed. The Fukui model for minimum noise figure is expressed as

$$NFmin = 1 + 2\pi KfC_{gs}\sqrt{(R_g + R_s)/g_m} \times 10^{-3} \quad (1)$$

where, K, f, and C_{gs} are fitting parameter, frequency, gate-source capacitance, respectively. In [33], a more accurate model for the NFmin is defined as

$$NFmin = 1 + \beta C_{gs}\sqrt{S_{i_d^2}/g_m^2} \quad (2)$$

where, β is the fitting parameter. $S_{i_d^2}$ is the power spectral density of the channel noise and is expressed as

$$S_{i_d^2} = \frac{4kT}{I_D L}\int_{Vs}^{Vd} g(V)\ dV \quad (3)$$

where, I_D and L are the drain current and channel length, respectively.k and T are Boltzmann constant and temperature, respectively. Vs, Vd and $g(V)$ are potential on source side, potential on drain side and channel conductivity, respectively. From (1) to (3), it could be noted that the NFmin is a function of intrinsic and extrinsic parameters. Impact of these parameters on the device noise is discussed as follows. In general, the increase in gate width results in an increased C_{gs}, R_g and g_m. Also, increasing the gate-width causes a reduction in R_s. Eq. 1 shows that the NFmin is directly proportional to C_{gs}, R_g, R_s; while it is inversely proportional to g_m. In [3], the NFmin was shown to increase as the gate width increases. It is further identified using Eq. (1) and NFmin in [3] that the increase in the gate width significantly increases (or influences) the NFmin through C_{gs} and R_g rather than g_m and R_s. The reason behind this identification has not been proved yet and need to be proved in future. This is a research gap in the design of LNA system. Furthermore, the noise is inversely proportional to g_m and L_g. On the other hand, g_m is inversely proportional to L_g. Therefore, the g_m contradicts with L_g on the proportionality with NFmin. Due to these contradictions, more details and intensive investigation are required to efficiently identify the noise sources in GaN HEMT.

III. DEVICE SCHEMATIC AND SIMULATION APPROACH

The schematic diagram of the investigated AlGaN/GaN HEMT is shown in Fig. 2. This device is constructed using TCAD physical simulator. The device consists of 22-nm AlGaN barrier layer and 3 μm GaN epi-layer. In order to protect the ambient contaminant, Silicon Nitride (SiN) is used as a passivation layer and Silicon Carbide is used as a substrate. The device has a unit-gate-width of 50 μm and 8 fingers (8×50 μm). The gate-length (L_G), gate-source spacing (L_{GS}) and gate-drain spacing (L_{GD}) are 0.25 μm, 1 μm and 2.7 μm, respectively [34]. In order to improve the reliability of simulation, various physics-based models were used to accurately characterize the device physics. Shockley-Read-Hall (SRH) recombination model is used to facilitate the carrier generation and recombination in the device. A field dependent mobility model is used to limit the carrier transport beyond knee voltage. The drift-diffusion, continuity and poison's equation are default models in TCAD simulator. These models are used to govern the carrier transport and dynamics in performed simulations. The GaN region is partitioned into two regions such as GaN channel and GaN buffer. In GaN channel and AlGaN barrier, intrinsic doping (1×10^{15} cm^{-3}) is used. In GaN buffer, acceptors are used with a concentration of 5×10^{16} cm^{-3} to mimic the buffer traps [29]. The energy level of the buffer traps is 0.5eV below the channel. Newton's method [35] is used to solve the physics based models over numerous rectangular cells of GaN-HEMT.

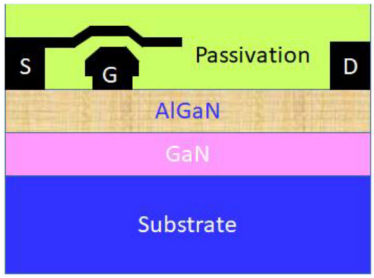

FIGURE 2. Schematic diagram of the GaN HEMT on SiC substrate with source field plate.

In the case of the DC simulation, the terminal voltages are swept and the terminal currents are observed. In the case of the RF and noise simulation, the device is considered as a two-port network. The RF signal is given as input with varying frequencies. The input and the output ports are terminated with a 50 Ω resistor. Initially, DC solutions (setting the gate and the drain bias) are solved, then the bias-based physics are saved in the physical model; while the RF solutions are solved. During the AC analysis, majority and minority carriers (electrons and holes) are enabled in the numerical method. During the RF analysis, the frequency is swept at a fixed gate and drain bias. The simulator outputs the capacitance and admittance matrices. Using these matrices, the S-parameters are extracted as input reflection coefficient (S_{11}), output reflection coefficient (S_{22}), reverse gain (S_{12}) and forward gain (S_{21}).

IV. RESULT AND DISCUSSION

The measured and simulated transfer characteristic of GaN HEMT on SiC substrate is shown in Fig. 3. The specification of the measured device [34] that were implemented in the TCAD simulation is given in Table 1. As shown from the results in Fig. 3, the device pinch-off at gate voltage of −3 V. As shown, the simulation result fits very well with the measured data. Furthermore, the simulated transconductance fits well with measured data as shown in Fig. 4. The simulated output characteristics shown in Fig. 5, also show a very good fitting of simulated results with the measured data. This ensures the validity of the DC simulation in TCAD.

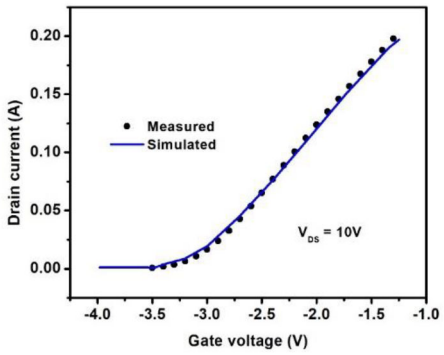

FIGURE 3. Simulated and measured transfer characteristics of 8×50-μm GaN-on-SiC HEMT at V_{DS} =10V.

TABLE 1. Specification of the measured device.

Parameter	Dimension	Parameter	Dimension
Gate length	0.25 µm	AlGaN thickness	22 nm
Gate-drain distance	2.7 µm	GaN thickness	3 µm
Gate-source distance	1 µm	Substrate thickness	100 µm

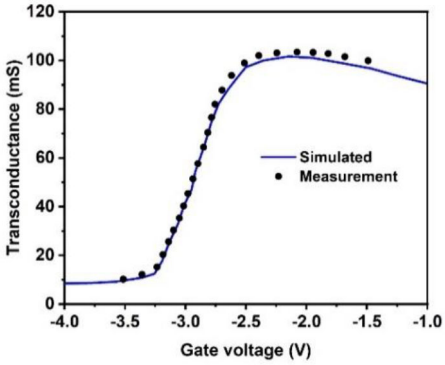

FIGURE 4. Simulated and measured transconductance at V_{DS} = 10V.

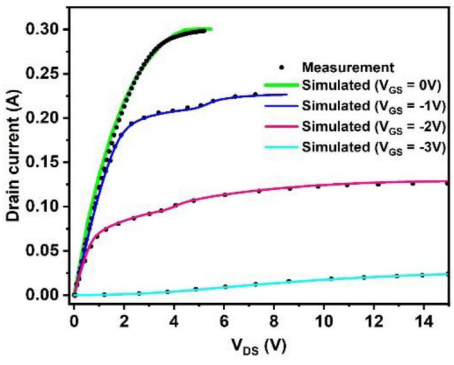

FIGURE 5. Simulated and measured output characteristics of 8×50-μm GaN-on-SiC HEMT.

Apart from validating the DC simulation results, the simulated S-parameters and noise parameters have been also validated. Fig. 6 shows the input reflection coefficient (S_{11}) and output reflection coefficient (S_{22}) of the GaN HEMT.

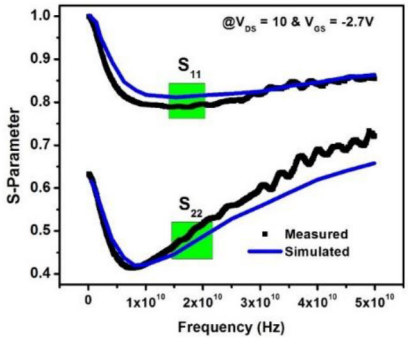

FIGURE 6. Measured and simulated S_{11} and S_{22} of 8×50-μm GaN-on-SiC HEMT.

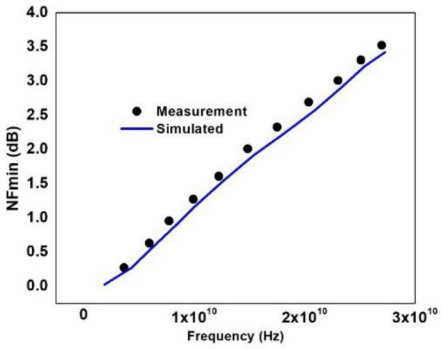

FIGURE 7. Simulated and measured NFmin of 8×50-μm GaN-on-SiC HEMT at V_{DS} = 10V and V_{GS} = −2.7V.

The simulated S_{11} and S_{22} show very good agreement with the measurements. This establishes the accuracy of the physical model used in this study. Also, the validation of S-parameter simulation in rectangular plot is preferred as it captures the resonance behaviour of the device. This resonance behaviour of S-parameter in smith chart is not visible. Fig. 7 shows simulated and measured NFmin at $V_{DS} = 10$V and $V_{GS} = -2.7$V. Both simulated and measured noise figures have a very good agreement and linearly increase with frequency.

Fukui [36] demonstrated that the minimum noise figure is inversely proportional to transconductance. In order to verify this, the transconductance of the device is analyzed. The transconductance for various AlGaN barrier thicknesses (t_{AlGaN}) at a drain voltage of 10 V is shown in Fig. 8. It is observed that the peak value of the tranconductance increases when t_{AlGaN} is decreased. This is attributed to the proximity of the gate to the channel for lower AlGaN barrier thickness.

The threshold voltage also decreases when t_{AlGaN} is decreased. This is attributed to the reduction of conduction band offset (ΔE_C) or quantum well depth [37] as t_{AlGaN} decreases. The transconductance, as shown in Fig. 8, is divided into region I and region II. This region split is done to show the dependency of the transconductance on the gate voltage. In region I, at particular gate bias, the

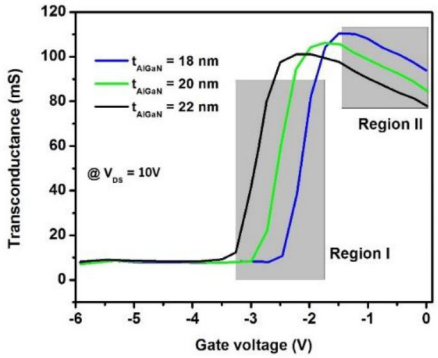

FIGURE 8. Transconductance for various AlGaN thickness at $V_{DS} = 10V$.

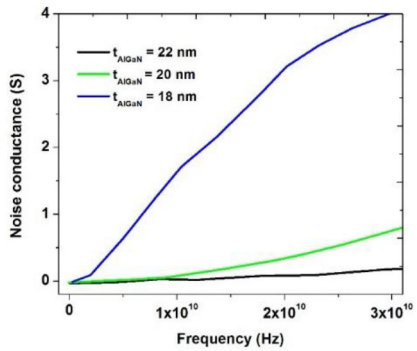

FIGURE 9. Noise conductance at $V_{DS} = 10$ v and $V_{GS} = -2.7V$.

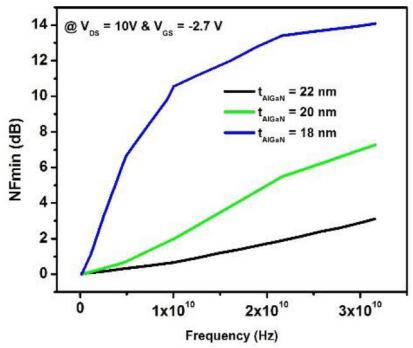

FIGURE 10. NFmin for different AlGaN thickness at $V_{DS} = 10V$ and $V_{GS} = -2.7V$.

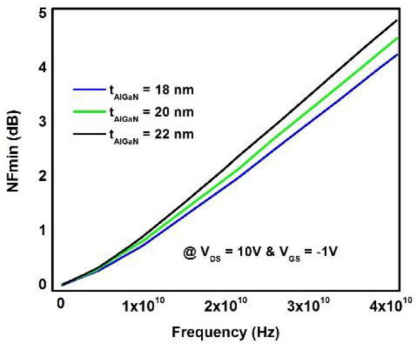

FIGURE 11. NFmin for different AlGaN thicknesses at $V_{DS} = 10V$ and $V_{GS} = -1V$.

transconductance is higher for higher AlGaN thickness. In region II, the transconductance is higher for lower AlGaN thickness. Therefore, the gate bias point of lower AlGaN thickness (18 nm) in GaN based LNA has to be in region II. The observed transconductance phenomena are related to the minimum noise figure, as will be explained later.

In general, the noise in a semiconductor device is the fluctuation of conductance, and it is one of the important parameter in noise analysis [38]. Thus, the noise conductance is analysed with great detail in this study. The noise conductance is shown to be directly proportional to the microscopic current source or noise current [38]. This noise conductance behaviour is depicted in Fig. 9. At a gate bias of -2.7 V, the noise conductance increases decently as t_{AlGaN} decreases. A significant increase in noise conductance is observed for $t_{AlGaN} = 18$ nm compared to 20 nm and 22 nm. According to Pucel model [38], NFmin is directly proportional to noise conductance. Therefore, the variation of the NFmin with AlGaN thickness presented in Fig. 10 is consistent with the noise conductance shown in Fig. 9 and agrees well with the Pucel model. The minimum noise figure (NFmin) versus frequency for various t_{AlGaN}, shown in Fig. 10, is obtained at a drain bias of 10V and gate bias of -2.7. It is observed that the minimum noise figure increases as t_{AlGaN} decreases. This is consistent with the transconductance behaviour versus t_{AlGaN} shown in Fig. 8. It is noticeable that the observed increase in minimum noise becomes quite significant for $t_{AlGaN} = 18$ nm as compared to 20 nm and 22 nm.

As a result, it is suggested that high gate negative bias (closer to pinch-off voltage) is not recommended for low AlGaN thicknesses. Consequently, the minimum noise figure is then simulated at a gate voltage of -1V at various t_{AlGaN} and different frequencies. The simulation results are illustrated in Fig. 11. At first glance, one can observe that the minimum noise figure is less sensitive to the change in t_{AlGaN} (the effect of t_{AlGaN} change on NFmin values are minor as compared to the results shown in Fig. 10). This stems from the fact that the tranconductance is higher for lower t_{AlGaN} at $V_{GS} = -1V$ as revealed by the results shown in Fig. 8. It is also noteworthy to note that, unlike the behaviour shown in Fig. 10, a smaller t_{AlGaN} yields less NFmin for results obtained with $V_{GS} = -1V$ depicted in Fig. 11. In [8], it is stated that the increase of AlGaN barrier increases the NFmin. This is not true for all bias conditions (See Figs. 10 and 11). Therefore, we state that the impact of AlGaN barrier thickness on the NFmin depends on the gate bias voltage. The LNA is typically operated in class A, which can be implemented at a range of gate bias voltages. This also depends on the peak-to-peak voltage of LNA RF input signal. The use of lower gate bias for LNA improves its performance. Therefore, the bias condition has to be optimized according to the implemented AlGaN barrier thickness.

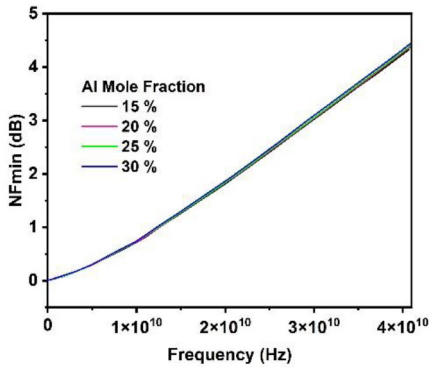

FIGURE 12. Minimum noise figure over the frequency for various Aluminium mole fraction (or Al Mole fraction) in AlGaN epitaxial barrier.

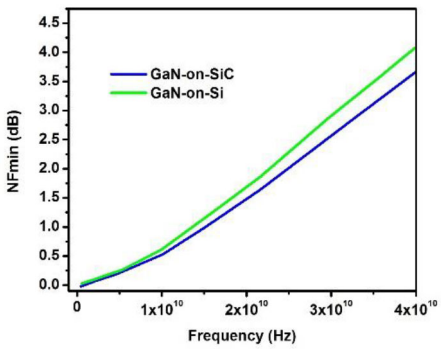

FIGURE 13. NFmin for Si and SiC substrate.

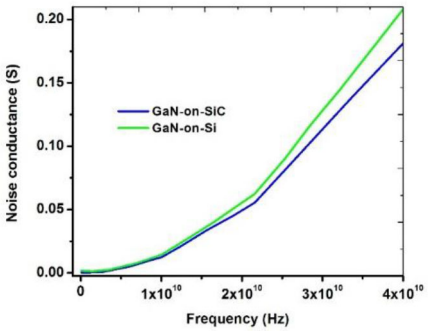

FIGURE 14. Noise conductance for Si and SiC substrate.

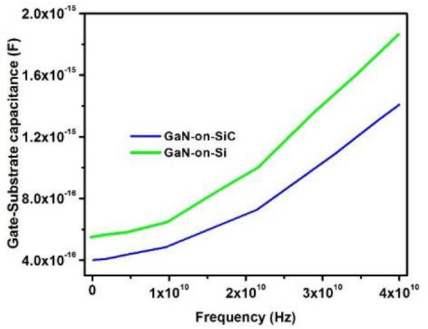

FIGURE 15. Gate to substrate capacitance for Si and SiC substrate.

Apart from the AlGaN barrier thickness, the Aluminum (Al) mole fraction in AlGaN barrier is varied and NFmin is observed. In [8], [19], the Al mole fraction was varied and its impact on the NFmin is observed. In [19] the experimental work showed that the NFmin is almost constant for the variation of Al mole fraction. In Fig. 12, we also observed that the NFmin is almost constant at different values of the Al mole fraction and consistent with the experimental data in [19]. This is an additional validation to TCAD simulation in this work. In [8], Al mole fraction is varied in AlGaN layer below the channel (not the AlGaN barrier) and it is TCAD simulation not validated with experimental data. This is also shown that NFmin increases with the increase of Al mole fraction of AlGaN layer below the channel. Therefore, the impact of Al mole fraction on NFmin in [8] needs further investigation to prove it.

Next the impact of the substrate material on NFmin is investigated. The investigated substrate materials are Silicon (Si) and Silicon Carbide (SiC). These substrates are chosen as they are competitive in terms of cost and performance and are commonly used. Fig. 13 shows the simulated NFmin for GaN-on-Si and GaN-on-SiC at gate bias of -2.7V. Initially, the TCAD simulation of GaN-on-SiC is validated with measurement and NFmin is observed. Then, the SiC is replaced by Si and its NFmin is benchmarked with SiC substrate. It is observed that GaN-on-Si yielded higher NFmin than that of GaN-on-SiC. This could be related to the higher leakage through the Si substrate as compared to SiC substrate [39].

The noise conductance (g_n) in GaN HEMT for Si and SiC substrates are shown in Fig. 14. Noise conductance is an indicator for the noise/leakage current in a semiconductor device. The noise conductance is expressed as [40]:

$$g_n = \frac{< i_d^2 >}{4kT} \tag{4}$$

where, i_d^2 is the drain noise current. In Fig. 14, the noise conductance for both devices is almost the same for frequencies below 10 GHz. However, for frequencies above 10 GHz, the noise conductance of Si substrate is higher than that of SiC. This is attributed to the lower resistivity ($\rho = 6.4 \times 10^2 \Omega$m) of Si substrate, which then induces higher leakage [41]. The phenomena of noise conductance (g_n) shown in Fig. 14 is consistent with Eq. (4) that g_n is proportional with drain noise current (or inversely proportional with resistivity). The higher noise conductance for Si substrate enhances the noise in GaN-on-Si device as revealed by Fig. 13.

One more important parameter, which is analyzed in this work, is the gate to substrate (C_{g-sub}) capacitance. The control of this parameter may improve the higher leakage in GaN HEMT for Si substrate. The gate-substrate capacitance for Si and SiC substrates are characterized by the stored charges around the buffer-substrate interface as shown in Fig. 15. It is evident that the C_{g-sub} for Si substrate is higher than

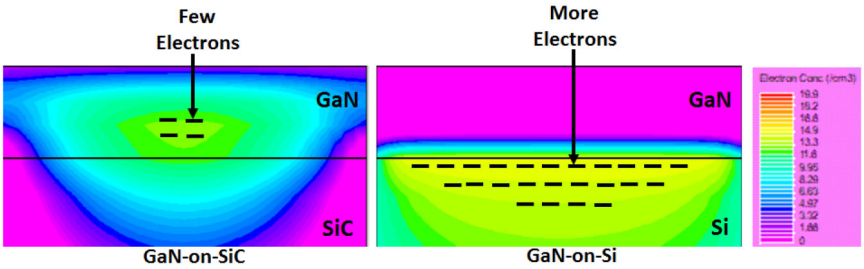

FIGURE 16. Electron concentration of GaN-on-SiC and GaN-on-Si calculated using TCAD. The gate length, unit-gate-width and number of gate fingers used in the TCAD simulation are 0.25 μm, 50 μm and 8, respectively.

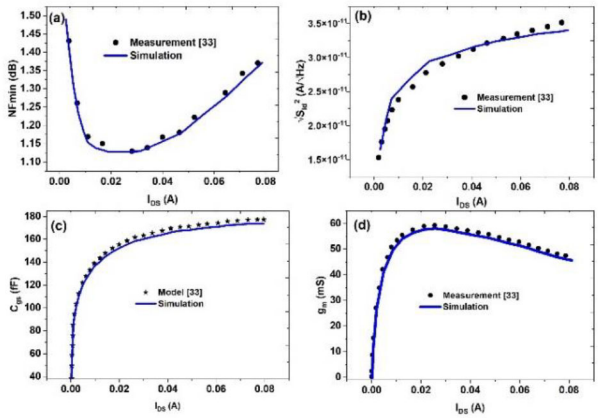

FIGURE 17. (a) NFmin, (b) drain noise current, (c) gate-source capacitance and (d) transconductance versus drain current at V_{DS} = 9V and a frequency of 9 GHz. The model and experimental data are reported in [33].

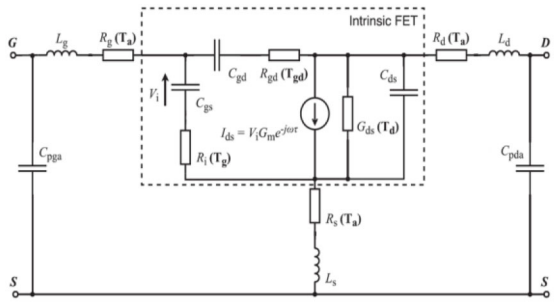

FIGURE 18. Small-signal equivalent circuit noise model for GaN HEMT.

that one for the SiC and this is caused by the higher stored charges for the Si substrate.

From Fig. 16, it is clear that the charge carrier in the substrate region for the Si-based device is higher compared to the GaN-on-SiC. This carrier is the basis for higher leakage in GaN on Si substrate. Even though the gate-substrate capacitance is used to demonstrate the presence of charges in Si substrate, the simulated carrier concentration is also calculated for better understanding of substrate related leakage phenomena. Fig. 16 shows the electron concentration for GaN-on-Si versus GaN-on-SiC. To provide better clarity, the region around GaN/substrate interface is shown in Fig. 16. It is interesting to note that the electron concentration at GaN/Si interface is higher than that of GaN/SiC interface. Overall, the electron concentration in the substrate region for GaN-on-Si is higher than that of GaN-on-SiC. The higher electrons concentration induces more leakage in the GaN-on-Si device.

For further validation of our TCAD simulation, we have simulated the experimental device reported in [33] and compared the simulated results to measurements. The gate width and gate length of the experimental device are 200 μm and 0.25 μm, respectively. In Fig. 17, NFmin, drain current noise (S_{id}^2), gate-source capacitance (C_{gs}) and transconductance over drain current are all depicted. V_{DS} and frequency are kept at 9 V and 9 GHz, respectively. The model data is obtained using Eq. (2) [33]. This model shows that the minimum noise figure (NFmin) is directly proportional to the gate-to-source capacitance (C_{gs}) and drain current noise, while it is inversely proportional to transconductance. As can be seen from Fig. 17, C_{gs} and S_{id}^2 are proportional to NFmin in the higher drain current region, hence, C_{gs} and S_{id}^2 will have an impact only on the NFmin at higher drain current. On the other hand, the NFmin is inversely proportional to g_m in the entire drain current region. Furthermore, the impact of g_m on the NFmin is also higher in the lower drain current region compared to the higher drain current region. The influence of transconductance on the NFmin is also verified using the small signal noise model shown in Fig. 18 and then compared to TCAD simulation. Small signal models are commonly used in analysing microwave amplifier designs.

The small signal model shown in Fig. 18 is used for the proposed design analysis as it represents the equivalent circuit of our experimental device. The flow of the process used in TCAD and the circuit simulation using ADS (Advanced Design System) CAD software is shown in Fig. 19.

The measured S-parameters and N-parameters are used to extract the design parameters of the model as listed in Table 2. The small-signal modelling and extraction procedures are reported elsewhere [3]. T_a and T_{gd} are assigned 297K value (ambient temperate). T_g and T_d are optimized for best fitting with the measured N-parameters [3] as illustrated in Fig. 20. The developed model is implemented in ADS simulator. Using ADS, the transconductance G_m is swept and its influence on NFmin is observed. The simulated NFmin

TABLE 2. Parameters of small-signal model at $V_{GS} = -2.72$ V and $V_{DS} = 10$ V.

Parameters	Value	Parameters	Value
L_g	156.1 pH	G_m	100 mS
L_s	11.26 pH	τ	2 psec
L_d	139.92 pH	C_{gs}	557.5 fF
R_g	0.88 Ω Ω	C_{gd}	85.7 fF
R_s	0.06 Ω	C_{ds}	165 fF
R_d	2.23 Ω	C_{pga}	27.2 fF
R_i	1.47 Ω	C_{pda}	28.56 fF
R_{gd}	2.09 Ω		

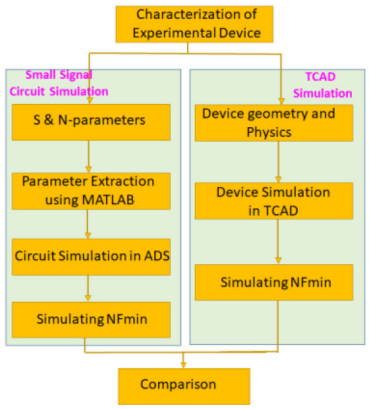

FIGURE 19. Flow of TCAD and small-signal circuit simulation.

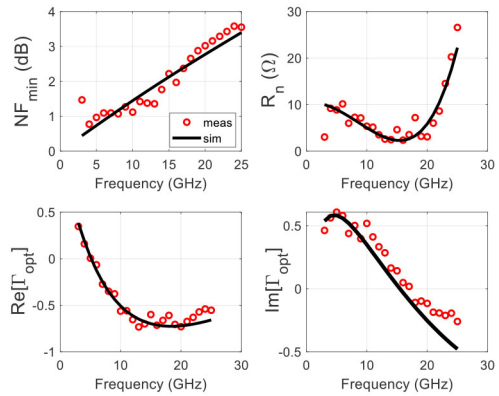

FIGURE 20. Measured (dotted) and simulated (solid) noise parameters of 8×50-μm GaN HEMT at $V_{GS} = -2.7$ V and $V_{DS} = 10$ V.

using ADS and TCAD are depicted in Fig. 20. In terms of trend, the NFmin obtained from the physical model in the TCAD and the small signal model are consistent. Both of them decrease with the increase in G_m values. In terms of numerical values, the NFmin of the physical device in TCAD simulation shows discrepancy as compared to the NFmin obtained from the small-signal model in ADS simulation. This discrepancy is attributed to the fact that the small signal model does not include the gate leakage noise [42] and the carrier generation/diffusion noise [29]; while TCAD physical device simulation consider all these noise sources. In this paper, investigation of the NFmin using TCAD physical device simulation as well as ADS circuit simulation is

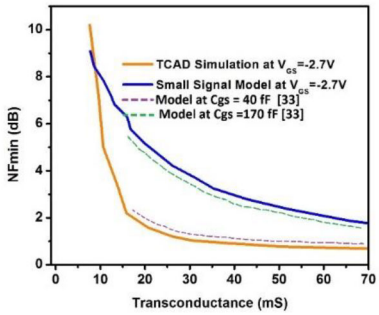

FIGURE 21. Simulated minimum noise figure versus transconductance using small-signal model in Advanced Design System (ADS) circuit simulator, physical device in TCAD simulator. The model data extracted using Eq. (1) for Cgs = 40 fF and Cgs = 170 fF [33].

TABLE 3. List of GaN based noise investigation.

Reference	TCAD Simulation	Model	Fabricated	Year
[20]			✓	1998
[24]			✓	1998
[25]			✓	2000
[49]		✓		2001
[51]			✓	2002
[23]			✓	2002
[47]			✓	2004
[19]			✓	2005
[48]			✓	2009
[30]		✓	✓	2009
[54]		✓		2010
[52]		✓		2012
[53]		✓		2013
[50]	✓	✓		2014
[46]		✓		2015
[12]			✓	2017
[22]			✓	2019
[31]			✓	2020
[3]		✓		2020
This work	✓			

used to establish the validity of the fact that the impact of g_m and substrate leakage on NFmin is significant.

To support our simulated results, Eq. (2) [33] is used with $C_{gs} = 40$ fF and 160 fF to calculate the model data shown in Fig. 21. It is interesting to note that the model with lower C_{gs} (40 fF) shows a good agreement with the physical device simulation in TCAD. On the other hand, the model with higher C_{gs} (160 fF) shows good agreement with the simulated results obtained using the small-signal model in ADS. This is because of counting inter-electrode and pad capacitances by the small signal model; while the TCAD model underestimates this capacitance. Therefore, based on the capacitance value, one can use the Eq. (2) to verify the TCAD simulation as well as the small signal model. Furthermore, the demonstration of noise performance assists the device and circuit designers for better noise performance of the LNA.

Compared to the GaAs technology and MESFET [38], [43], [44], [45], the noise based research in

GaN technology is lower. Our work is compared with state of the art of noise based research in GaN technology [1], [33], [47], [48], [49], [50], [51], [53], [54], which is given in Table 3. Based on the comparison, it is found that there is less work carried out in noise simulation of GaN HEMT using TCAD tool. This provides a cost-effective and fast approach to verify an idea in semiconductor devices. Also, the reliability of the TCAD model could be improved by calibration with experimental S-parameters and N-parameters measurements. This approach provides an efficient tool to predict the performance of the LNA in terms of device physics. Thus, in addition to the circuit design, the LNA performance could be improved at the device level by optimizing its physical parameters (geometry, material, and processing parameters).

V. CONCLUSION

In this paper, the impact of AlGaN barrier thickness and substrate material on the noise performance in GaN HEMT is investigated. The TCAD simulation is used to analyse the noise performance. It is observed that decreasing t_{AlGaN} increases the minimum noise figure at a higher negative gate bias. On the other hand, decreasing t_{AlGaN} will decrease the minimum noise figure at lower negative bias. Therefore, it is recommended to reduce the gate bias if t_{AlGaN} is reduced. Furthermore, the impact of the substrate material on the noise performance is analysed. It is found that the minimum noise figure for GaN-on-Si is higher than that of the GaN-on-SiC. This is due to the higher gate-to-substrate capacitance for GaN-on-Si. Further, simulation of physical device in TCAD and small signal model in ADS is performed and compared to show the impact of C_{gs} and g_m on noise. The presented procedure is very effective for optimizing the GaN HEMT physical parameters (structure, material and fabrication process) for improved noise characteristics. This in addition to the circuit topology could provide an efficient tool for optimal design of the LNA.

REFERENCES

[1] M. Rudolph, R. Doerner, E. Ngnintendem, and W. Heinrich, "Noise modeling of GaN HEMT devices," in *Proc. 7th Eur. Microw. Integr. Circuits Conf.*, Amsterdam, The Netherlands, Oct. 2012, pp. 159–162.

[2] S. Colangeli, A. Bentini, W. Ciccognani, and E. Limiti, "Polynomial noise modeling of silicon-based GaN HEMTs," *Int. J. Numer. Model.*, vol. 27, nos. 5–6, pp. 812–821, Sep. 2014.

[3] A. Jarndal, A. Hussein, G. Crupi, and A. Caddemi, "Reliable noise modeling of GaN HEMTs for designing low-noise amplifiers," *Int. J. Numer. Model.*, vol. 33, p. e2585, May/Jun. 2020.

[4] Z. Wu, S. Li, and B. Li, "High-frequency noise modeling of GAN HEMT with double recessed barrier layer," *Microw. Opt. Technol. Lett.*, vol. 64, no. 3, pp. 464–470, Mar. 2022.

[5] Y. J. Choi, J.-H. Lee, S. J. An, and K.-S. Im, "Low-frequency noise behavior of AlGaN/GaN HEMTs with different Al compositions," *Crystals*, vol. 10, no. 9, p. 830, Sep. 2020.

[6] G. Crupi, A. Raffo, V. Vadalà, G. Vannini, and A. Caddemi, "High-periphery GaN HEMT modeling up to 65 GHz and 200 °C," *Solid-State Electron.*, vol. 152, pp. 11–16, Feb. 2019.

[7] J.-S. Moon *et al.*, "360 GHz f_{MAX} graded-channel AlGaN/GaN HEMTs for mmW low-noise applications," *IEEE Electron Device Lett.*, vol. 41, no. 8, pp. 1173–1176, Aug. 2020.

[8] D. K. Panda and T. R. Lenka, "Device optimization of E-Mode N-Polar GaN MOS-HEMT for low noise RF and microwave applications," in *Proc. Int. Workshop Phys. Semicond. Devices*, New Delhi, India, Dec. 2017, pp. 171–176.

[9] K. Sinha, S. K. Dubey, and A. Islam, "Study of high Al fraction in AlGaN barrier HEMT and GaN and InGaN channel HEMT with $In_{0.17}Al_{0.83}N$ barrier," *Microsyst. Technol.*, vol. 26, pp. 2145–2158, Jul. 2020.

[10] Y.-S. Lin and S.-F. Lin, "Large-signal linearity and high-frequency noise of passivated AlGaN/GaN high-electron mobility transistors," *Micromachines*, vol. 12, no. 1, p. 7, Dec. 2021.

[11] R. Matthias, C. Andrei, R. Doerner, S. A. Chevtchenko, and W. Heinrich, "Noise in GaN HEMTs and circuits," in *Proc. Int. Conf. Noise Fluctuations*, Vilnius, Lithuania, Jun. 2017, pp. 1–4.

[12] C. Andrei, R. Doerner, S. A. Chevtchenko, W. Heinrich, and M. Rudolph, "On the optimization of GaN HEMT layout for highly rugged low-noise amplifier design," in *Proc. 12th Eur. Microw. Integr. Circuits Conf.*, Nuremberg, Germany, Dec. 2017, pp. 244–247.

[13] P. Aaen, J. Plá, and J. Wood, *Modeling and Characterization of RF and Microwave Power FETs*. Cambridge, U.K.: Cambridge Univ. Press, 2007.

[14] K. Sehra, V. Kumari, M. Gupta, M. Mishra, D. S. Rawal, and M. Saxena, "Optimization of π–Gate AlGaN/AlN/GaN HEMTs for low noise and high gain applications," *Silicon*, vol. 14, pp. 393–404, Jan. 2022.

[15] C. K. Maiti, *Introducing Technology Computer-Aided Design (TCAD) Fundamentals, Simulations, and Applications*. Singapore: Pan Stanford Publ. Pte. Ltd., 2017.

[16] D. S. Lee, X. Gao, S. Guo, D. Kopp, P. Fay, and T. Palacios, "300-GHz InAlN/GaN HEMTs with InGaN back barrier," *IEEE Electron Device Lett.*, vol. 32, no. 11, pp. 1525–1527, Nov. 2011.

[17] E. Bahat-Treidel, F. Brunner, O. Hilt, E. Cho, J. Wurfl, and G. Trankle, "AlGaN/GaN/GaN:C back-barrier HFETs with breakdown voltage of over 1 kV and low $R_{ON} \times A$," *IEEE Trans. Electron Devices*, vol. 57, no. 11, pp. 3050–3058, Nov. 2010.

[18] M. H. Wong *et al.*, "N-face metal–insulator–semiconductor high-electron-mobility transistors with AlN back-barrier," *IEEE Electron Device Lett.*, vol. 29, no. 10, pp. 1101–1104, Oct. 2008.

[19] C. Sanabria *et al.*, "Influence of epitaxial structure in the noise figure of AlGaN/GaN HEMTs," *IEEE Trans. Microw. Theory Techn.*, vol. 53, no. 2, pp. 762–769, Feb. 2005.

[20] M. E. Levinshtein, S. L. Rumyantsev, R. Gaska, J. W. Yang, and M. S. Shur, "AlGaN/GaN high electron mobility field effect transistors with low 1/f noise," *Appl. Phys. Lett.*, vol. 73, no. 8, pp. 1089–1091, Aug. 1998.

[21] S. L. Rumyantsev *et al.*, "Effect of gate leakage current on noise properties of AlGaN/GaN field effect transistors," *J. Appl. Phys.*, vol. 88, no. 11, p. 6726, Nov. 2000.

[22] K.-S. Ima *et al.*, "1/f noise characteristics of AlGaN/GaN HEMTs with periodically carbon-doped GaN buffer layer," *Microelectron. Eng.*, vol. 215, Jul. 2019, Art. no. 110985.

[23] S. A. Vitusevich *et al.*, "Excess low-frequency noise in AlGaN/GaN-based high-electron-mobility transistors," *Appl. Phys. Lett.*, vol. 80, no. 12, pp. 2126–2128, Mar. 2002.

[24] D. V. Kuksenkov, H. Temkin, R. Gaska, and J. W. Yang, "Low-frequency noise in AlGaN/GaN heterostructure field effect transistors," *IEEE Electron Device Lett.*, vol. 19, no. 7, pp. 222–224, Jul. 1998.

[25] J. A. Garrido *et al.*, "Low-frequency noise and mobility fluctuations in AlGaN/GaN heterostructure field-effect transistors," *Appl. Phys. Lett.*, vol. 76, no. 23, pp. 3442–3444, May 2000.

[26] A. Balandin, "Gate-voltage dependence of low-frequency noise in GaN/AlGaN heterostructure field-effect transistors," *Electron. Lett.*, vol. 36, no. 10, pp. 912–913, May 2000.

[27] L. K. J. Vandamme and F. N. Hooge, "What do we certainly know about $1/f$ noise in MOSTs?" *IEEE Trans. Electron Devices*, vol. 55, no. 11, pp. 3070–3085, Nov. 2008.

[28] E. Burstein, R. H. Kingston, and A. L. McWhorter, *Semiconductor Surface Physics*. Philadelphia, PA, USA: Univ. Pennsylvania Press, 1957.

[29] N. K. Subramani, "Physics-based TCAD device simulations and measurements of GaN HEMT technology for RF power amplifier applications," Ph.D. dissertation, Dept. Electronics, Université de Limoges, Limoges, France, 2017.

[30] Z. H. Liu, S. Arulkumaran, and G. I. Ng, "Improved microwave noise performance by SiN passivation in AlGaN/GaN HEMTs on Si," *IEEE Microw.Wireless Compon. Lett.*, vol. 19, no. 6, pp. 383–385, Jun. 2009.

[31] T. Huang, O. Axelsson, J. Bergsten, M. Thorsell, and N. Rorsman, "Impact of AlGaN/GaN interface and passivation on the robustness of low-noise amplifiers," *IEEE Trans. Electron Devices*, vol. 67, no. 6, pp. 2297–2303, Jun. 2020.

[32] W. Lee, D. Han, W. Choi, and B. Sarlioglu, "Reducing reverse conduction and switching losses in GaN HEMT-based high-speed permanent magnet brushless DC motor drive," in *Proc. IEEE Energy Conv. Congr. Expo.*, Cincinnati, OH, USA, 2017, pp. 3522–3528.

[33] A. Dasgupta, S. Khandelwal, and Y. S. Chauhan, "Surface potential based modeling of thermal noise for HEMT circuit simulation," *IEEE Microw. Wireless Compon. Lett.*, vol. 25, no. 6, pp. 376–378, Jun. 2015.

[34] D. Floriot *et al.*, "GH25-10: New qualified power GaN HEMT process from technology to product overview," in *Proc. 9th Eur. Microw. Integr. Circuit Conf.*, Rome, Italy, 2014, pp. 225–228.

[35] *Device Simulator Atlas Ver. 5.10.0.R. Atlas User's Manual*, Silvaco Int., Santa Clara, CA, USA, Jul. 2005.

[36] H. Fukui, "Optimal noise figure of microwave GaAs MESFET's," *IEEE Trans. Electron Devices*, vol. ED-26, no. 7, pp. 1032–1037, Jul. 1979.

[37] S. Sharbati, I. Gharibshahian, T. Ebel, A. A. Orouji, and W.-T. Franke, "Analytical model for two-dimensional electron gas charge density in recessed-gate GaN high-electron-mobility transistors," *J. Electron. Mater.*, vol. 50, pp. 3923–3929, Apr. 2021.

[38] R. A. Pucel, H. A. Haus, and H. Statz, "Signal and noise properties of gallium arsenide microwave field-effect transistors," *Adv. Electron. Electron Phys.*, vol. 38, pp. 195–265, Jan. 1975.

[39] A. Jarndal, A. Z. Markos, and G. Kompa, "Improved modeling of GaN HEMTs on Si substrate for design of RF power amplifiers," *IEEE Trans. Microw. Theory Techn.*, vol. 59, no. 3, pp. 644–651, Mar. 2011.

[40] B. Carnez, A. Cappy, R. Fauquembergue, E. Constant, and G. Salmer, "Noise modeling in submicrometer-gate FET's," *IEEE Trans. Electron Devices*, vol. 28, no. 7, pp. 784–789, Jul. 1981.

[41] A. Jarndal L. Arivazhagan, and D. Nirmal, "On the performance of GaN-on-silicon, silicon-carbide, and diamond substrates," *Int. J. RF Microw. Comput.-Aided Eng.*, vol. 30, no. 12, Jun. 2020, Art. no. e22196.

[42] V. Rizzoli, F. Mastri, and C. Cecchetti, "Computer-aided noise analysis of MESFET and HEMT mixers," *IEEE Trans. Microw. Theory Techn.*, vol. 37, no. 9, pp. 1401–1410, Sep. 1989.

[43] P. Heymann and M. Rudolph, *A Guide to Noise in Microwave Circuits: Devices, Circuits and Measurement*. Newark, NJ, USA: Wiley, 2021.

[44] M. W. Pospiezalski, "Modeling of noise parameters of MESFETs and MODFETs and their frequency and temperature dependence," *IEEE Trans. Microw. Theory Tech.*, vol. 37, no. 9, pp. 1340–1350, Sep. 1989.

[45] V. Guru *et al.*, "Analytical noise model of a high-electron-mobility transistor for microwave-frequency application," *Microw. Optoelectr. Technol. Lett.*, vol. 40, no. 5, pp. 410–417, Mar. 2004.

[46] J.-W. Lee, A. Kuliev, V. Kumar, R. Schwindt, and I. Adesida, "Microwave noise characteristics of AlGaN/GaN HEMTs on SiC substrates for broad-band low-noise amplifiers," *IEEE Microw. Wireless Compon. Lett.*, vol. 14, no. 6, pp. 259–261, Jun. 2004.

[47] M. Thorsell, K. Andersson, M. Fagerlind, M. Sudow, P.-A. Nilsson, and N. Rorsman, "Thermal study of the high-frequency noise in GaN HEMTs," *IEEE Trans. Microw. Theory Techn.*, vol. 57, no. 1, pp. 19–26, Jan. 2009.

[48] C. H. Oxley, "Calculation of minimum noise figure using the simple Fukui equation for gallium nitride (GaN) HEMTs," *Solid-State Electron.*, vol. 45, no. 5, pp. 677–682, May 2001.

[49] A. Dasgupta, S. Khandelwal, and Y. S. Chauhan, "Compact modeling of Flicker noise in HEMTs," *IEEE J. Electron Devices Soc.*, vol. 2, no. 6, pp. 174–178, Nov. 2014.

[50] J. S. Moon *et al.*, "Microwave noise performance of AlGaN-GaN HEMTs with small DC power dissipation," *IEEE Electron Device Lett.*, vol. 23, no. 11, pp. 637–639, Nov. 2002.

[51] S. Colangeli, W. Ciccognani, E. Limiti, and A. Bentini, "Polynomial noise modeling of silicon-based GaN HEMTs," *Int. J. Numer. Model.: Electron. Netw.*, vol. 27, nos. 5–6, pp. 812–821, May 2013.

[52] Z. H. Liu, G. I. Ng, and S. Arulkumaran, "Analytical modeling of high-frequency noise including temperature effects in GaN HEMTs on high-resistivity Si substrates," *IEEE Trans. Electron Devices*, vol. 57, no. 7, pp. 1485–1491, Jul. 2010.